LA-UR-11-04542

Approved for public release;
distribution is unlimited.

Title:	Comparison of Discrete and Continuous Thermal Neutron Scattering Cross-Section Treatments in MCNP5
Author(s):	A.T. Pavlou, F.B. Brown, W.R. Martin, B.C. Kiedrowski
Intended for:	MCNP References

Form 836 (7/06)

Comparison of Discrete and Continuous Thermal Neutron Scattering Cross-Section Treatments in MCNP5

A.T. Pavlou, F.B. Brown*, W.R. Martin, B.C. Kiedrowski*

The University of Michigan–Ann Arbor

Department of Nuclear Engineering & Radiological Sciences

2355 Bonisteel Boulevard, Ann Arbor, MI 48109, USA

atpavlou@umich.edu, wrm@umich.edu

*Los Alamos National Laboratory

X-Computational Physics Division, Monte Carlo Codes Group

P.O. Box 1663, MS A143

Los Alamos, NM 87545, USA

fbrown@lanl.gov, bckiedro@lanl.gov

Abstract

The standard discrete thermal neutron scattering treatment in MCNP5 is compared with a continuous scattering treatment using a criticality suite of 119 benchmark cases. In the analysis, six bound isotopes are considered: beryllium metal, graphite, hydrogen in water, hydrogen in polyethylene, beryllium in beryllium oxide and oxygen in beryllium oxide. Overall, there are small changes in the eigenvalue (k_{eff}) between discrete and continuous treatments with the largest differences being greater than three standard deviations for a mixed-oxide (MOX) lattice with borated water at 1090.4 ppm and an unreflected spherical reactor containing uranyl-nitrate solution. The results indicate the changes in eigenvalue between continuous and discrete treatments are random, small and well within the uncertainty of measured data for reactor criticality experiments.

Key Words: criticality, nuclear data, validation, benchmarks

1 Introduction and Background

The cross section for bound isotopes varies depending on the material being bound to. The bound and free gas cross sections are the same at high energies, but vary in the thermal energy range ($< 4\ eV$). In this thermal energy range, scattering events can occur resulting in a gain or loss in energy from interactions with the target material. This is because of the comparable energies between the neutron and the target [1] that allows energy transfer from the target to the neutron and vice versa. This complicates the physics of the scattering process and the calculation of the scattering cross section. Depending on the target material, neutrons will scatter coherently or incoherently, and a large amount of computer memory is needed to store this scattering information. The scattering events are described by changes in the neutron momentum (α) [2,3],

$$\alpha = \frac{(\vec{p} - \vec{p'})^2}{2mAkT}, \tag{1}$$

and neutron energy (β),

$$\beta = \frac{E - E'}{kT}, \tag{2}$$

where energy and momentum are dependent on one another. Also, α and β are dimensionless quantities. In these equations, $\vec{p}$ and $\vec{p'}$ are, respectively, the pre- and post-collision neutron momentum vectors, m is the neutron mass, A is the mass of the scattering atom (the ratio of the target mass and the neutron mass), kT is the ambient temperature, E and E' are, the pre- and post-collision neutron energies and μ is the cosine of the scattering angle. The double-differential scattering cross section in the thermal scattering region [4] is commonly expressed in terms of α and β by

$$\sigma(E \to E', \mu) = \frac{\sigma_b}{2kT}\sqrt{\frac{E'}{E}} \exp\left(-\frac{\beta}{2}\right) S(\alpha, \beta), \tag{3}$$

where σ_b is the cross section of the bound atom. The bound atom cross section is related to the free atom cross section (σ_{free}) by [5]

$$\sigma_b = \left(1 + \frac{1}{A}\right)^2 \sigma_{\text{free}}, \tag{4}$$

Currently, Monte Carlo codes such as MCNP5 [6] use an $S(\alpha, \beta)$ treatment to describe scattering events in the thermal region for some materials. This S function stores a large majority of the scattering physics and is thus referred to as the scattering law. The current discrete method stores values of the $S(\alpha, \beta)$ function for particular values of α and β. This is done by expressing the double-differential downscattering probability distribution function (pdf) by a product of the marginal pdf, $m(\beta \mid E)$, and conditional pdf, $c(\alpha \mid \beta, E)$, in alpha, beta and initial energy [7,8]:

$$f(\alpha,\beta) = \frac{\sigma(\alpha,\beta)}{\int_0^{E/kT} d\beta' \int_{\alpha_{min}}^{\alpha_{max}} d\alpha' \sigma(\alpha',\beta')} = \left[\frac{\int_{\alpha_{min}}^{\alpha_{max}} d\alpha' \sigma(\alpha',\beta')}{\int_0^{E/kT} d\beta' \int_{\alpha_{min}}^{\alpha_{max}} d\alpha' \sigma(\alpha',\beta')} \right] \cdot \left[\frac{\sigma(\alpha,\beta)}{\int_{\alpha_{min}}^{\alpha_{max}} d\alpha' \sigma(\alpha',\beta')} \right], \tag{5}$$

where

$$\left[\frac{\int_{\alpha_{min}}^{\alpha_{max}} d\alpha' \sigma(\alpha',\beta')}{\int_0^{E/kT} d\beta' \int_{\alpha_{min}}^{\alpha_{max}} d\alpha' \sigma(\alpha',\beta')} \right] = m(\beta \mid E), \tag{6}$$

$$\left[\frac{\sigma(\alpha,\beta)}{\int_{\alpha_{min}}^{\alpha_{max}} d\alpha' \sigma(\alpha',\beta')} \right] = c(\alpha \mid \beta, E), \tag{7}$$

and α_{min} and α_{max} are the lower and upper limits, respectively, of Eq.(1) found by setting the cosine of the scattering angle, μ, equal to 1 and -1, respectively [9]. Hence,

$$\alpha_{min} = \frac{(\sqrt{E} - \sqrt{E'})^2}{AkT}, \tag{8}$$

$$\alpha_{max} = \frac{(\sqrt{E} + \sqrt{E'})^2}{AkT}. \tag{9}$$

In Eq.(5), $\int_0^{E/kT} d\beta' \int_{\alpha_{min}}^{\alpha_{max}} d\alpha' \sigma(\alpha',\beta')$ represents the total downscattering cross section at E. By knowing the initial neutron energy, the first bracketed term on the right-hand side of Eq.(5) is integrated from 0 to β and set equal to a random number, thus determining a value for β. The same procedure is used to determine α from the other distribution function, knowing the initial neutron energy and the energy transfer β from the first sample. The process is repeated for neutron upscattering by refining the terms in Eq.(5) using the principle of detailed balance. The result is a discrete energy and a discrete direction for

the collided neutron. The disadvantage of the current discrete method is the presence of residual spikes that occur at the low energy cutoff. While this typically is not a problem for reactor problems, certain applications require a more accurate, continuous treatment of the thermal scattering law.

To model the physics of thermal scattering more accurately, a method was developed by Bob MacFarlane [10] that uses a continuous-energy distribution. The secondary energy distributions are converted into pdf form and stored. For an incident energy, a script determines the closest energy stored in the file. Next, the cumulative distribution function (cdf) data is searched for the sample and the outgoing energy is interpolated from the pdf and cdf. Angles are then sampled from the distribution using the initial and final energies. These continuous $S(\alpha, \beta)$ cross sections were developed for a select number of isotopes.

2 Results

To test the effect of using discrete versus continuous $S(\alpha, \beta)$ cross sections in MCNP5, a criticality validation suite of 119 benchmark problems developed by Russell Mosteller [11] is used. The benchmarks are divided into five major categories based on the isotope that provides the majority of fission: Uranium-233, High-Enriched Uranium (HEU), Intermediate-Enriched Uranium (IEU), Low-Enriched Uranium (LEU) and Plutonium.

The continuous $S(\alpha, \beta)$ cross sections are specified in the MCNP inputs using an XS card, which reads cross-section data for the defined isotope from a specified location outside the standard *xsdir* file. The continuous $S(\alpha, \beta)$ datasets are obtained from the *t2.lanl.gov* website. These files were generated by Bob MacFarlane using NJOY with ENDF/B-VII.0 data in October 2007. All other materials are evaluated using the ENDF/B-VII.0 library. The materials in the benchmarks that are affected by the $S(\alpha, \beta)$ treatment are hydrogen in water, hydrogen in polyethylene, beryllium metal, beryllium in beryllium oxide, oxygen in beryllium oxide, and graphite. Of the 119 benchmarks, 64 use $S(\alpha, \beta)$ thermal scattering treatments. Therefore, only these 64 benchmarks are discussed.

There is very little change in the eigenvalue between the two treatments, with the largest change being around 160 pcm[1]. This 160 pcm change in eigenvalue occurs in a MOX lattice with fuel rods contained in borated water at 1090.4 ppm (bolded in Table 1). Similar benchmarks are tested with the same parameters, but with less boron. These cases are described in Table 1 and displayed in Fig.1 in order of decreasing boron concentration. The dotted red line represents no change in the eigenvalue between treatments.

The errors reported in the tables have been rounded to preserve significant digits. The actual unrounded errors are reflected in the figures. All analyses of the data have been performed using the unrounded errors.

[1]pcm = per cent mille, or one-thousandth of a percent.

Table 1: Pacific Northwest Laboratory (PNL) MOX Benchmark Parameters and Eigenvalue Results*

Case Number	Fuel Rods	Pitch [cm]	Soluble Boron [ppm]	Experiment k_{eff}	Discrete k_{eff}	Continuous k_{eff}	Δk from Discrete
106	469	1.77800	1.7	1.0024(60)	1.0010(3)	1.0017(3)	0.0007(4)
107	761	1.77800	687.9	1.0009(47)	1.0028(3)	1.0024(3)	-0.0004(4)
108	195	2.20914	0.9	1.0042(31)	1.0032(3)	1.0026(3)	-0.0006(4)
109	**761**	**2.20914**	**1090.4**	**1.0024(21)**	**1.0079(3)**	**1.0063(3)**	**-0.0016(4)**
110	161	2.51447	1.6	1.0038(25)	1.0046(3)	1.0040(3)	-0.0006(4)
111	689	2.51447	767.2	1.0029(27)	1.0068(3)	1.0063(3)	-0.0005(4)
	RMS Error				0.00726	0.00567	
	RMS Continuous / RMS Discrete				0.78080		

*The use of parenthesis represents standard deviation times a factor of 10^4. For example, 0.0007(4) is equivalent to 0.0007 +/- 0.0004.

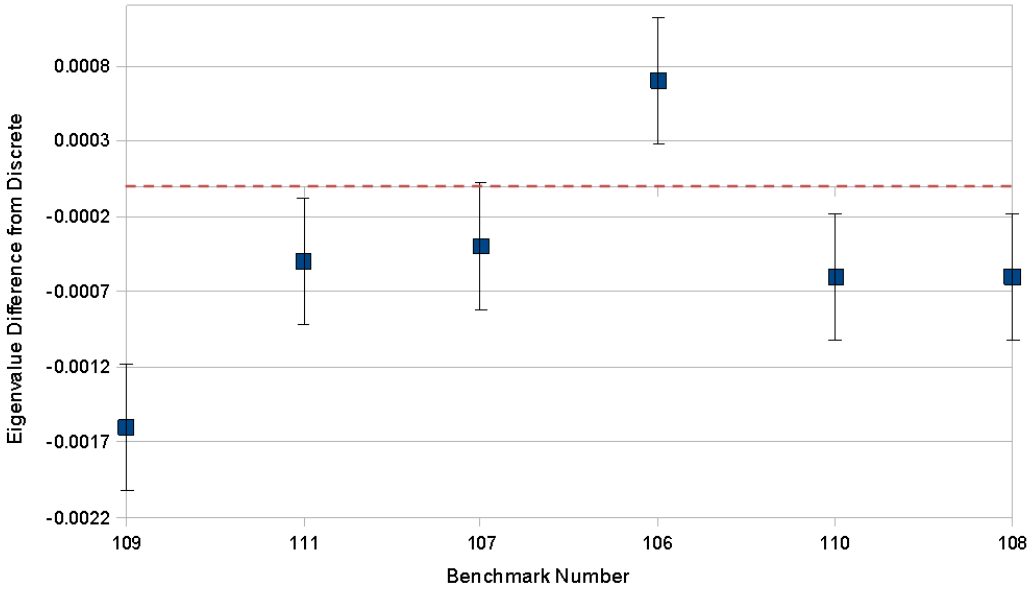

Figure 1: Deviation of Continuous Eigenvalue Results from Discrete for Pacific Northwest Laboratory (PNL) MOX Benchmarks

For the most part, as the amount of boron is decreased in the water, the change in eigenvalue between continuous and discrete $S(\alpha, \beta)$ treatments for water also decreases. This makes sense since one expects large differences when changing the scattering law for the scattering material (hydrogen in water) as the amount of the scattering material is being reduced in the system. However, a definitive pattern could not be determined. The MOX lattice benchmark case 106 with 1.7 ppm of boron shows an increase in eigenvalue when a continuous $S(\alpha, \beta)$ treatment is used whereas all other MOX lattice benchmarks show a decrease.

The uncertainty in the difference between discrete and continuous eigenvalues is determined using standard error propagation, where the two values are assumed to be uncorrelated. Therefore, the uncertainty in the difference of discrete and continuous eigenvalues is proportional to the square root of the sum of the squares of the individual uncertainties,

$$\delta_{\Delta k} = \sqrt{\left(\frac{\partial(\Delta k)}{\partial k_{\text{eff},d}}\right)^2 \delta^2_{k_{\text{eff},d}} + \left(\frac{\partial(\Delta k)}{\partial k_{\text{eff},c}}\right)^2 \delta^2_{k_{\text{eff},c}}}, \tag{10}$$

where $\delta_{\Delta k}$ is the standard deviation of the difference of discrete and continuous eigenvalues, $k_{\text{eff},d}$ and $k_{\text{eff},c}$ are the eigenvalue results from the discrete cross-section treatment and continuous cross-section treatment, respectively, and $\delta_{k_{\text{eff},d}}$ and $\delta_{k_{\text{eff},c}}$ are the standard deviations of the discrete eigenvalue and continuous eigenvalue results, respectively.

The root-mean-square error (RMS) is computed for the discrete and continuous cases, each being compared to their respective experimental result. The RMS error for the discrete treatment is given by

$$\varepsilon = \sqrt{\sum_i (k_{\text{eff},d,i} - k_{\text{eff},e,i})^2}, \tag{11}$$

where $k_{\text{eff},d,i}$ and $k_{\text{eff},e,i}$ are the eigenvalue results for the i^{th} benchmark for the discrete treatment and the experimental case, respectively. The RMS error for the continuous treatment is the same as Eq.(11), but with the discrete eigenvalue replaced by the continuous eigenvalue. The RMS error shows on average how far the uncertainty deviates from zero. By dividing the *Continuous RMS Error* by the *Discrete RMS Error*, an assessment of the affect of the continuous $S(\alpha, \beta)$ treatment can be made. The closer this ratio is to unity, the closer the two treatments are to one another.

Tables 2–6 and Figs.2–6 show the eigenvalue differences between the two scattering cross section treatments for different groups of benchmark problems. To emphasize the significant results, eigenvalue differences of less than one standard deviation have been omitted (accounts for 27 of the 64 thermal-treated cases). A full list of results can be found in the appendix. Results that differ by more than three standard deviations have been bolded and italicized. All cases were run using 10,000 source histories per cycle with 600 cycles, the first 100 of which were discarded.

Table 2: U233 Benchmark Eigenvalue Results

Case Number	Experiment k_{eff}	Discrete k_{eff}	Continuous k_{eff}	Δk from Discrete
14	1.0000(33)	1.0011(3)	1.0015(3)	0.0004(4)
15	1.0000(33)	1.0009(3)	1.0005(3)	-0.0004(4)
16	**1.0000(33)**	**1.0019(3)**	**1.0006(3)**	**-0.0013(4)**
17	1.0000(33)	0.9996(3)	1.0000(3)	0.0004(4)
18	1.0000(29)	1.0014(2)	1.0011(2)	-0.0003(3)
	RMS Error	0.00278	0.00202	
	RMS Continuous / RMS Discrete	0.72468		

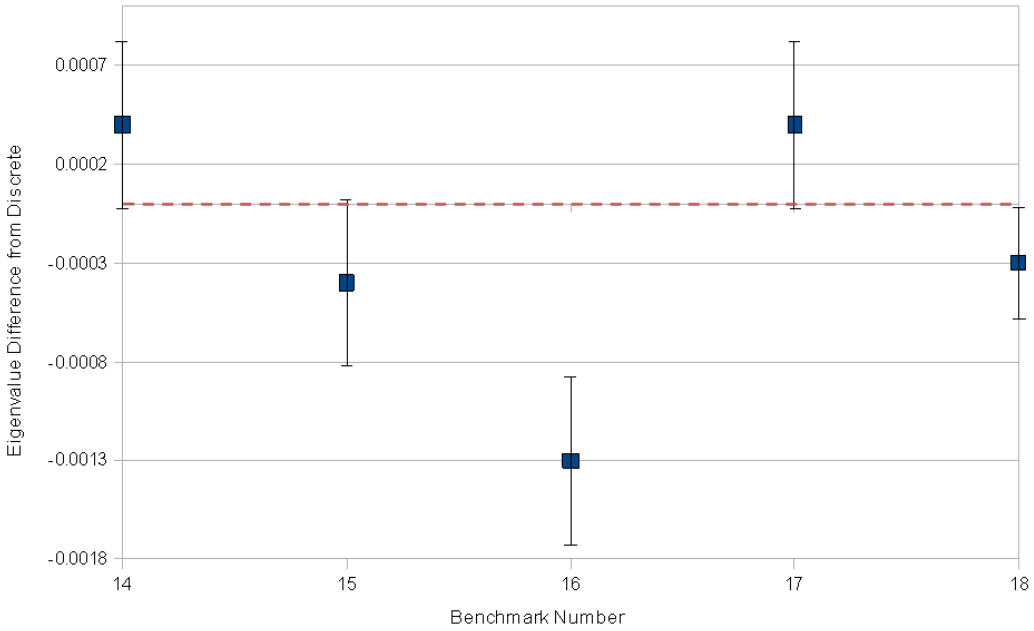

Figure 2: Deviation of Continuous Eigenvalue Results from Discrete for U233 Benchmarks

Table 3: HEU Benchmark Eigenvalue Results

Case Number	Experiment k_{eff}	Discrete k_{eff}	Continuous k_{eff}	Δk from Discrete
42	0.9992(15)	0.9957(3)	0.9951(3)	-0.0006(4)
43	0.9989(15)	0.9989(2)	0.9983(3)	-0.0006(4)
50	0.9977(8)	0.9960(3)	0.9970(3)	0.0010(4)
53	1.0015(28)	1.0000(4)	1.0009(4)	0.0009(6)
54	1.0012(26)	0.9985(3)	0.9989(3)	0.0004(4)
56	1.0009(36)	0.9942(3)	0.9938(3)	-0.0004(4)
58	1.0015(26)	0.9991(2)	0.9994(2)	0.0003(3)
	RMS Error	0.00868	0.00884	
	RMS Continuous / RMS Discrete	1.01842		

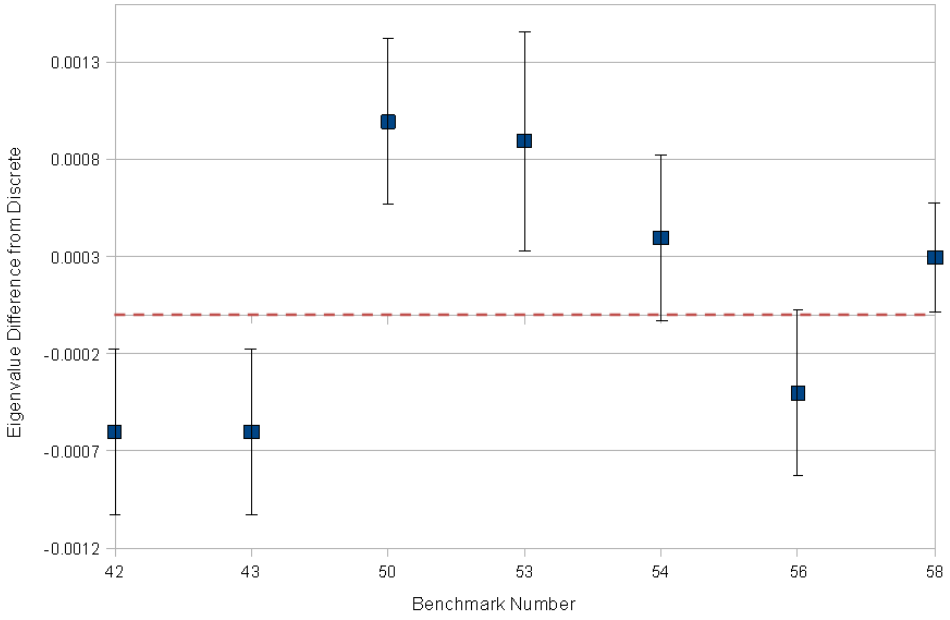

Figure 3: Deviation of Continuous Eigenvalue Results from Discrete for HEU Benchmarks

Table 4: IEU Benchmark Eigenvalue Results

Case Number	Experiment k_{eff}	Discrete k_{eff}	Continuous k_{eff}	Δk from Discrete
70	1.0017(44)	1.0041(3)	1.0034(3)	-0.0007(4)
71	0.9961(9)	0.9950(3)	0.9955(3)	0.0005(4)
72	0.9973(9)	0.9977(3)	0.9971(3)	-0.0006(4)
73	0.9985(10)	0.9958(3)	0.9963(3)	0.0005(4)
74	0.9988(11)	0.9986(3)	0.9991(3)	0.0005(4)
	RMS Error	0.00380	0.00287	
	RMS Continuous / RMS Discrete	0.75397		

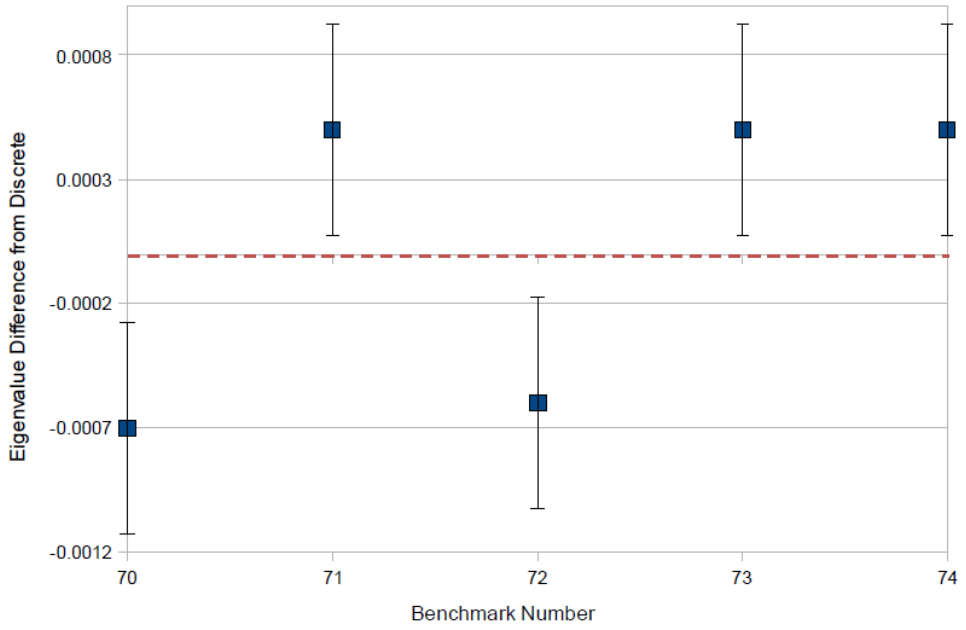

Figure 4: Deviation of Continuous Eigenvalue Results from Discrete for IEU Benchmarks

Table 5: LEU Benchmark Eigenvalue Results

Case Number	Experiment k_{eff}	Discrete k_{eff}	Continuous k_{eff}	Δk from Discrete
76	1.0007(16)	1.0012(3)	1.0005(3)	-0.0007(4)
79	1.0007(16)	1.0003(3)	0.9999(3)	-0.0004(4)
80	1.0007(16)	1.0007(3)	1.0000(3)	-0.0007(4)
81	1.0007(16)	1.0020(3)	1.0014(3)	-0.0006(4)
83	1.0024(37)	0.9959(3)	0.9951(3)	-0.0008(4)
	RMS Error	0.00666	0.00741	
	RMS Continuous / RMS Discrete	1.11311		

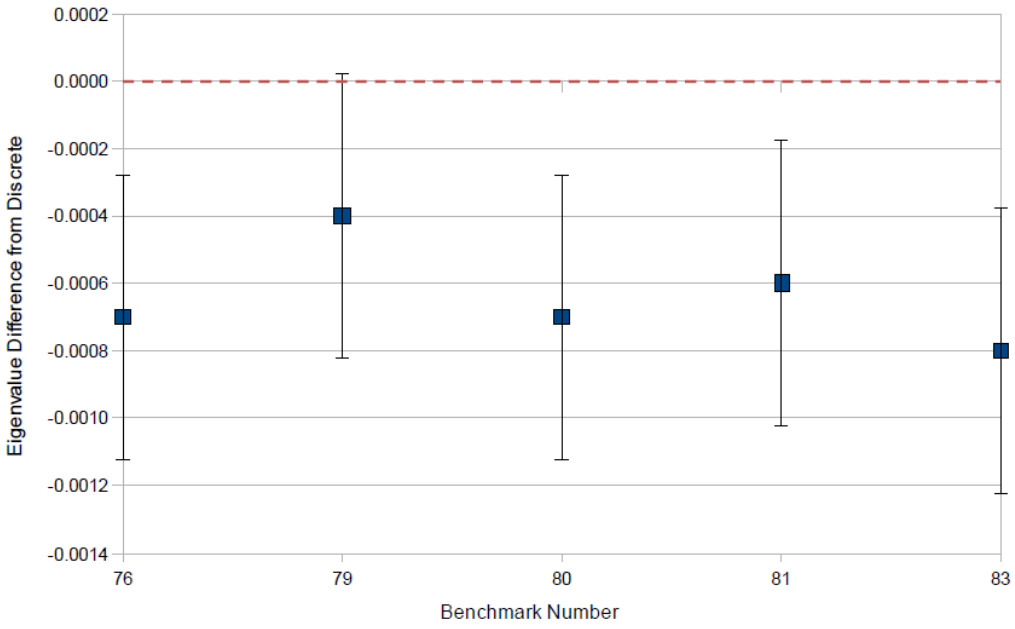

Figure 5: Deviation of Continuous Eigenvalue Results from Discrete for LEU Benchmarks

Table 6: Pu Benchmark Eigenvalue Results

Case Number	Experiment k_{eff}	Discrete k_{eff}	Continuous k_{eff}	Δk from Discrete
99	0.9992(15)	0.9975(3)	0.9979(3)	0.0004(4)
100	1.0000(20)	1.0019(3)	1.0024(3)	0.0005(4)
101	1.0000(10)	1.0006(3)	1.0001(3)	-0.0005(4)
102	1.0000(26)	0.9931(3)	0.9922(3)	-0.0009(4)
103	1.0000(26)	1.0021(3)	1.0033(3)	0.0012(4)
105	1.0000(110)	1.0116(2)	1.0119(2)	0.0003(3)
106	1.0024(60)	1.0010(3)	1.0017(3)	0.0007(4)
107	1.0009(47)	1.0028(3)	1.0024(3)	-0.0004(4)
108	1.0042(31)	1.0032(3)	1.0026(3)	-0.0006(4)
109	**1.0024(21)**	**1.0079(3)**	**1.0063(3)**	**-0.0016(4)**
110	1.0038(25)	1.0046(3)	1.0040(3)	-0.0006(4)
111	1.0029(27)	1.0068(3)	1.0063(3)	-0.0005(4)
115	1.0000(52)	0.9996(4)	1.0002(4)	0.0006(6)
117	1.0000(65)	1.0044(5)	1.0037(5)	-0.0007(7)
118	1.0000(34)	1.0031(3)	1.0026(3)	-0.0005(4)
	RMS Error	0.01659	0.01653	
	RMS Continuous / RMS Discrete	0.99665		

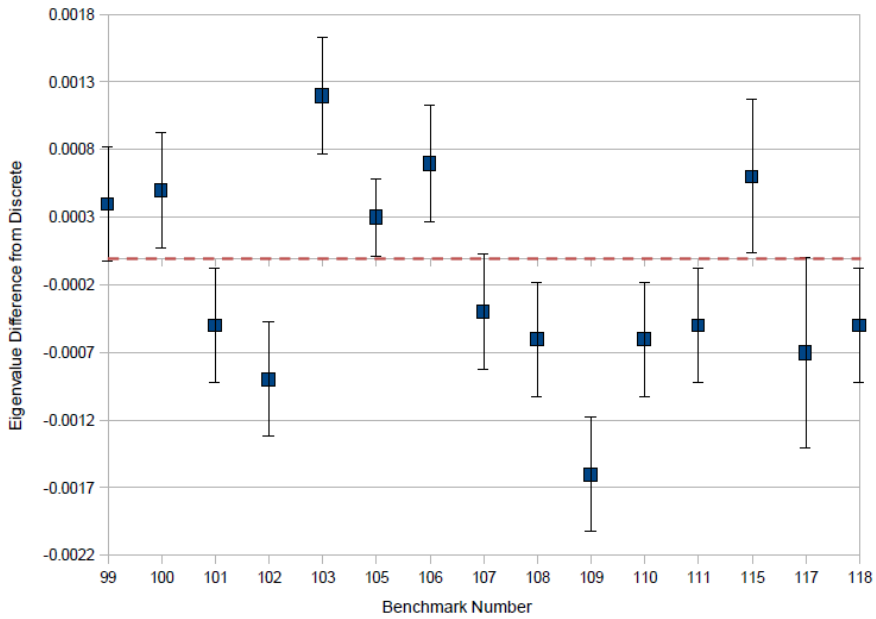

Figure 6: Deviation of Continuous Eigenvalue Results from Discrete for Pu Benchmarks

For three benchmark groups (U233, LEU and Pu), the RMS error for the continuous treatment is larger than that for the discrete treatment. The other two benchmark groups (HEU and IEU) show a decrease in RMS error for the continuous treatment.

Based on the results of the 37 cases discussed, approximately 14% (5 cases) yield an absolute eigenvalue difference between the discrete treatment and the continuous treatment of more than two standard deviations, with two of these five cases having a difference greater than three standard deviations.

The total RMS data for all 64 cases is given in Table 7.

Table 7: Total RMS for 64 Thermal Scattering-Treated Benchmarks

	Discrete	Continuous
Total RMS Error	0.03838	0.03857
Total RMS Continuous / Total RMS Discrete	1.00488	

From Table 7, there is no significant difference in the RMS error between discrete and continuous thermal scattering treatments when comparing all benchmark cases. The large RMS differences in Tables 2, 4 and 5 are a result of random fluctuations in the eigenvalue for individual cases. Because these groups of benchmarks contain a small number of cases, the RMS error is easily inflated by large eigenvalue differences in one or two cases.

3 Analysis of Benchmarks Yielding Large Eigenvalue Differences

Of the 64 benchmark cases affected by thermal scattering, two yield an eigenvalue difference greater than three standard deviations. These cases are analyzed further to determine a possible cause for the large deviation.

3.1 Benchmark Case 16: u233-sol-therm-001-case-4

This benchmark case is an unreflected, spherical reactor containing a solution of $U(NO_3)_2$ (uranyl-nitrate) inside an annular shell of Aluminum-1100 with a spherical source. The scattering material of interest for this benchmark problem is hydrogen in water. The five benchmark cases u233-sol-therm-001-case-1 through u233-sol-therm-001-case-5 all contain these same parameters with the concentration of uranyl-nitrate increasing for each case, from 17.14 g/l for case one to 19.82 g/l for case five. There does not appear to be a direct correlation between uranyl-nitrate concentration and the effect on eigenvalue through a different thermal scattering cross section treatment. The eigenvalue differences from the discrete cases appear to fluctuate randomly between the five cases.

This case is rerun for the continuous treatment using 100,000 source histories per cycle to see the reduction in the standard deviation. The eigenvalue yielded from this was 1.0009(1). Comparing this to the original result of 1.0006(3) using 10,000 source histories per cycle, one notices that the standard deviation decreases as expected, but the results do not significantly change because there is agreement between the two within the given uncertainty.

3.2 Benchmark Case 109: mix-comp-therm-002-case-pnl33

This benchmark case is a MOX lattice with fuel rods contained in borated water at 1090.4 ppm. The analysis of this case was done earlier in this document with the relevant parameters and results given in Table 1. For cases mix-comp-therm-002-case-pnl30 through mix-comp-therm-002-case-pnl35, a definitive trend could not be established relating the eigenvalue differences to the amount of borated water in the benchmark.

Similarly to benchmark case 16, this case is rerun for the continuous treatment using 100,000 source histories per cycle to see the reduction in the standard deviation. The eigenvalue yielded from this is 1.0069(1). Comparing this to the original result of 1.0063(3) using 10,000 source histories per cycle, one notices that the standard deviation decreases as expected and the results do not agree with each other within the given uncertainties. However, the change is still relatively small and insignificant.

4 Conclusions

There is a relatively small change in the eigenvalue when comparing discrete and continuous thermal scattering treatments with the largest difference being 160 pcm for a MOX lattice benchmark. The changes in eigenvalue between other benchmark cases do not appear to follow a pattern with each other. The changes are small, random and well within the uncertainty of measured data for reactor criticality experiments. This is because in reactor criticality experiments, only integrated values of the detailed thermal flux spectrum are of importance and the sharp edges resulting from discrete energy and angle pairs are not observed. In some non-reactor experiments with very few scatters or experiments where the detailed thermal flux spectrum is important, these sharp spikes need to be resolved and this is done through the continuous thermal scattering treatment. Therefore, although the continuous treatment is a more realistic, high-fidelity treatment of thermal scattering, further analyses with experiments consisting of a few scattering events are needed to justify a change from discrete to continuous treatment for future versions of MCNP. However, a change from the traditional discrete treatment to a continuous treatment does not significantly affect the results of criticality experiments.

REFERENCES

1. Weston M. Stacey, *Nuclear Reactor Physics, Second Edition*, (Wiley-VCH, 2007).

2. F.G. Bischoff, M.L. Yeater and W.E. Moore, "Monte Carlo Evaluation of Multiple Scattering and Resolution Effects in Double-Differential Neutron Scattering Cross-Section Measurements," *Nuclear Science and Engineering:* ***48****, 266-280* (1972).

3. Felix C. Difilippo and John P. Renier, "Double Differential Neutron Scattering Cross Sections of Materials for Ultra High Temperature Reactors," *Annals of Nuclear Energy:* ***34****, 130-139* (2007).

4. T.M. Sutton, T.H. Trumbull and C.R. Lubitz, "Comparison of Some Monte Carlo Models for Bound Hydrogen Scattering," *International Conference on Mathematics, Computational Methods & Reactor Physics*, Saratoga Springs, New York USA (2009).

5. D.E. Cullen, L.F. Hansen, E.M. Lent and E.F. Plechaty, *Thermal Scattering Law Data: Implementation and Testing Using the Monte Carlo Neutron Transport Codes COG, MCNP and TART*, UCRL-ID-153656, Lawrence Livermore National Laboratory (2003).

6. X-5 Monte Carlo Team, *MCNP—A General Monte Carlo N-Particle Transport Code, Version 5*, LA-UR-03-1987, Los Alamos National Laboratory (2003).

7. K.B. Cady, Personal Memo, March 30, 1966.

8. H. Lichtenstein, *et al.*, "The SAM-CE Monte Carlo System for Radiation Transport and Criticality Calculations in Complex Configurations," EPRI Computer Code Manual CCM-8 (1979).

9. C.T. Ballinger, "The Direct $S(\alpha, \beta)$ Method for Thermal Neutron Scattering," *Proc. Int. Conf. on Mathematics and Computation, Reactor Physics, and Environmental Analysis,* ***1***, 134, Portland, Oregon USA, April 30-May 4 (1995).

10. Bob MacFarlane, E-mail to Forrest Brown, March 9, 2006.

11. Russell Mosteller, *An Expanded Criticality Validation Suite for MCNP*, LA-UR-10-06230, Los Alamos National Laboratory (2010).

APPENDIX

The following tables display the eigenvalue results of discrete and continuous thermal scattering treatments as well as the differences between the two. RMS errors are also given to show deviations from the experimental results.

Table A1: U233 Benchmark Eigenvalue Results

Case Number	$S(\alpha,\beta)$-treated Isotope	Experiment k_{eff}	Discrete k_{eff}	Continuous k_{eff}	Δk from Discrete
9	Be Metal	1.0000(30)	0.9944(3)	0.9944(3)	0.0000(4)
10	Be Metal	1.0000(30)	0.9925(3)	0.9928(3)	0.0003(4)
11	H in H_2O	1.0000(83)	0.9848(5)	0.9844(5)	-0.0004(7)
12	H in H_2O / H in CH_2	1.0000(24)	1.0045(5)	1.0044(4)	-0.0001(6)
13	H in H_2O	1.0000(31)	1.0015(3)	1.0017(3)	0.0002(4)
14	H in H_2O	1.0000(33)	1.0011(3)	1.0015(3)	0.0004(4)
15	H in H_2O	1.0000(33)	1.0009(3)	1.0005(3)	-0.0004(4)
16	**H in H_2O**	**1.0000(33)**	**1.0019(3)**	**1.0006(3)**	**-0.0013(4)**
17	H in H_2O	1.0000(33)	0.9996(3)	1.0000(3)	0.0004(4)
18	H in H_2O	1.0000(29)	1.0014(2)	1.0011(2)	-0.0003(3)
	RMS Error		0.00278	0.00202	
	RMS Continuous / RMS Discrete		0.72468		

Table A2: HEU Benchmark Eigenvalue Results

Case Number	$S(\alpha,\beta)$-treated Isotope	Experiment k_{eff}	Discrete k_{eff}	Continuous k_{eff}	Δk from Discrete
40	Graphite	1.0000(28)	1.0073(3)	1.0073(3)	0.0000(4)
41	O in BeO / Be in BeO	0.9992(15)	0.9955(3)	0.9955(3)	0.0000(4)
42	Be Metal	0.9992(15)	0.9957(3)	0.9951(3)	-0.0006(4)
43	H in CH_2	0.9989(15)	0.9989(3)	0.9983(3)	-0.0006(4)
44	H in CH_2	1.0000(28)	1.0008(3)	1.0005(3)	-0.0003(4)
45	H in H_2O	1.0020(10)	1.0028(3)	1.0029(3)	0.0001(4)
47	H in CH_2	1.0000(38)	1.0037(3)	1.0037(3)	0.0000(4)
49	Graphite	0.9977(8)	0.9930(3)	0.9928(3)	-0.0002(4)
50	Graphite	0.9977(8)	0.9960(3)	0.9970(3)	0.0010(4)
51	Graphite	1.0015(9)	1.0006(3)	1.0004(3)	-0.0002(4)
52	Graphite	1.0016(8)	1.0075(3)	1.0073(3)	-0.0002(4)
53	H in H_2O / H in CH_2	1.0015(28)	1.0000(4)	1.0009(4)	0.0009(6)
54	H in H_2O	1.0012(26)	0.9985(3)	0.9989(3)	0.0004(4)
55	H in H_2O	1.0007(36)	0.9975(3)	0.9973(3)	-0.0002(4)
56	H in H_2O	1.0009(36)	0.9942(3)	0.9938(3)	-0.0004(4)
57	H in H_2O	1.0003(36)	0.9957(3)	0.9959(3)	0.0002(4)
58	H in H_2O	1.0015(26)	0.9991(2)	0.9994(2)	0.0003(3)
	RMS Error		0.01604	0.01598	
	RMS Continuous / RMS Discrete		0.99630		

Table A3: IEU Benchmark Eigenvalue Results

Case Number	$S(\alpha,\beta)$-treated Isotope	Experiment k_{eff}	Discrete k_{eff}	Continuous k_{eff}	Δk from Discrete
62	Graphite	1.0000(30)	1.0075(3)	1.0075(3)	0.0000(4)
70	H in H_2O	1.0017(44)	1.0041(3)	1.0034(3)	-0.0007(4)
71	H in H_2O	0.9961(9)	0.9950(3)	0.9955(3)	0.0005(4)
72	H in H_2O	0.9973(9)	0.9977(3)	0.9971(3)	-0.0006(4)
73	H in H_2O	0.9985(10)	0.9958(3)	0.9963(3)	0.0005(4)
74	H in H_2O	0.9988(11)	0.9986(3)	0.9991(3)	0.0005(4)
75	H in H_2O	0.9983(11)	0.9975(3)	0.9977(3)	0.0002(4)
	RMS Error		0.00845	0.00805	
	RMS Continuous / RMS Discrete		0.95322		

Table A4: LEU Benchmark Eigenvalue Results

Case Number	$S(\alpha,\beta)$-treated Isotope	Experiment k_{eff}	Discrete k_{eff}	Continuous k_{eff}	Δk from Discrete
76	H in H_2O	1.0007(16)	1.0012(3)	1.0005(3)	-0.0007(4)
77	H in H_2O	1.0007(16)	1.0013(3)	1.0015(3)	0.0002(4)
78	H in H_2O	1.0007(16)	1.0007(3)	1.0005(3)	-0.0002(4)
79	H in H_2O	1.0006(16)	1.0003(3)	0.9999(3)	-0.0004(4)
80	H in H_2O	1.0007(16)	1.0007(3)	1.0000(3)	-0.0007(4)
81	H in H_2O	1.0007(16)	1.0020(3)	1.0014(3)	-0.0006(4)
82	H in H_2O	1.0038(40)	1.0000(3)	0.9998(3)	-0.0002(4)
83	H in H_2O	1.0024(37)	0.9959(3)	0.9951(3)	-0.0008(4)
	RMS Error		0.00768	0.00846	
	RMS Continuous / RMS Discrete		1.10247		

Table A5: Pu Benchmark Eigenvalue Results

Case Number	$S(\alpha,\beta)$-treated Isotope	Experiment k_{eff}	Discrete k_{eff}	Continuous k_{eff}	Δk from Discrete
97	Graphite	1.0000(20)	0.9993(3)	0.9993(3)	0.0000(4)
98	Be Metal	1.0000(30)	0.9964(3)	0.9962(3)	-0.0002(4)
99	Be Metal	0.9992(15)	0.9975(3)	0.9979(3)	0.0004(4)
100	H in CH_2	1.0000(20)	1.0019(3)	1.0024(3)	0.0005(4)
101	H in H_2O	1.0000(10)	1.0006(3)	1.0001(3)	-0.0005(4)
102	O in BeO / Be in BeO	1.0000(26)	0.9931(3)	0.9922(3)	-0.0009(4)
103	Be Metal	1.0000(26)	1.0021(3)	1.0033(3)	0.0012(4)
105	Graphite	1.0000(110)	1.0116(2)	1.0119(2)	0.0003(3)
106	H in H_2O	1.0024(60)	1.0010(3)	1.0017(3)	0.0007(4)
107	H in H_2O	1.0009(47)	1.0028(3)	1.0024(3)	-0.0004(4)
108	H in H_2O	1.0042(31)	1.0032(3)	1.0026(3)	-0.0006(4)
109	**H in H_2O**	**1.0024(21)**	**1.0079(3)**	**1.0063(3)**	**-0.0016(4)**
110	H in H_2O	1.0038(25)	1.0046(3)	1.0040(3)	-0.0006(4)
111	H in H_2O	1.0029(27)	1.0068(3)	1.0063(3)	-0.0005(4)
112	H in H_2O	1.0000(33)	1.0190(2)	1.0189(2)	-0.0001(4)
113	H in H_2O	1.0000(52)	1.0060(4)	1.0061(4)	0.0001(6)
114	H in H_2O	1.0000(52)	0.9943(4)	0.9939(4)	-0.0004(6)
115	H in H_2O	1.0000(52)	0.9996(4)	1.0002(4)	0.0006(6)
116	H in H_2O	1.0000(32)	1.0043(4)	1.0048(4)	0.0005(6)
117	H in H_2O	1.0000(65)	1.0044(5)	1.0037(5)	-0.0007(7)
118	H in H_2O	1.0000(34)	1.0031(3)	1.0026(3)	-0.0005(4)
119	H in H_2O	1.0000(62)	0.9999(4)	0.9998(4)	-0.0001(6)
	RMS Error		0.02714	0.02726	
	RMS Continuous / RMS Discrete		1.00431		